HHS Public Access

Author manuscript

J Mol Cell Cardiol. Author manuscript; available in PMC 2017 July 01.

Published in final edited form as:

J Mol Cell Cardiol. 2016 July ; 96: 63–71. doi:10.1016/j.yjmcc.2015.07.030.

Atrial-selective targeting of arrhythmogenic phase-3 early afterdepolarizations in human myocytes

Stefano Morotti[a], **Andrew D. McCulloch**[b], **Donald M. Bers**[a], **Andrew G. Edwards**[c,d], and **Eleonora Grandi**[a,@]

[a]Department of Pharmacology, University of California Davis, Davis, CA, USA

[b]Department of Bioengineering, University of California San Diego, La Jolla, CA, USA

[c]Institute for Experimental Medicine, Oslo University Hospital Ullevål, Oslo, Norway

[d]Simula Research Laboratory, Lysaker, Norway

Abstract

Background—We have previously shown that non-equilibrium Na^+ current (I_{Na}) reactivation drives isoproterenol-induced phase-3 early afterdepolarizations (EADs) in mouse ventricular myocytes. In these cells, EAD initiation occurs secondary to potentiated sarcoplasmic reticulum Ca^{2+} release and enhanced Na^+/Ca^{2+} exchange (NCX). This can be abolished by tetrodotoxin-blockade of I_{Na}, but not ranolazine, which selectively inhibits ventricular late I_{Na}.

Aim—Since repolarization of human atrial myocytes is similar to mouse ventricular myocytes in that it is relatively rapid and potently modulated by Ca^{2+}, we investigated whether similar mechanisms can evoke EADs in human atrium. Indeed, phase-3 EADs have been shown to re-initiate atrial fibrillation (AF) during autonomic stimulation, which is a well-recognized initiator of AF.

Methods—We integrated a Markov model of I_{Na} gating in our human atrial myocyte model. To simulate experimental results, we rapidly paced this cell model at 10 Hz in the presence of 0.1 μM acetylcholine and 1 μM isoproterenol, and assessed EAD occurrence upon return to sinus rhythm (1 Hz).

Results—Cellular Ca^{2+} loading during fast pacing results in a transient period of hypercontractility after return to sinus rhythm. Here, fast repolarization and enhanced NCX facilitate I_{Na} reactivation via the canonical gating mode (i.e., not late I_{Na} burst mode), which drives EAD initiation. Simulating ranolazine administration reduces atrial peak I_{Na} and leads to faster repolarization, during which I_{Na} fails to reactivate and EADs are prevented.

Corresponding author: Eleonora Grandi, Department of Pharmacology, University of California Davis, 451 Health Sciences Drive, GBSF rm 3502, Davis, CA 95616. ; Email: ele.grandi@gmail.com Phone: (530) 752-4334 Fax: (530) 752-7710

DISCLOSURES

None.

Conclusions—Non-equilibrium I_{Na} reactivation can critically contribute to arrhythmias, specifically in human atrial myocytes. Ranolazine might be beneficial in this context by blocking peak (not late) atrial I_{Na}.

Graphical abstract

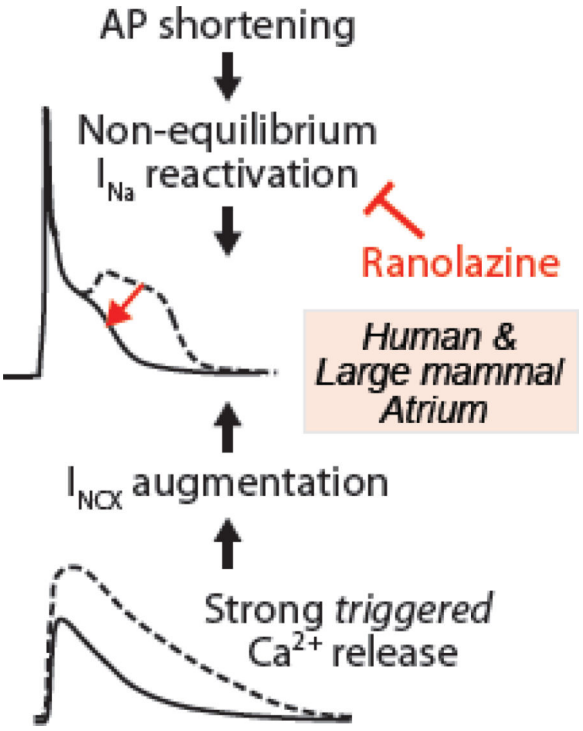

Keywords

Na^+ current; phase-3 EAD; atrial fibrillation; ranolazine; computer model

INTRODUCTION

Early afterdepolarizations (EADs) are abnormal depolarizations of cardiac myocyte membrane potential (E_m) occurring during phase-2 or phase-3 of the action potential (AP). EADs have been implicated as primary mechanisms promoting ventricular arrhythmias, including Torsades des Pointes, polymorphic ventricular tachycardia and ventricular fibrillation [1]. In ventricular cells from large mammals EADs generally occur in conditions of prolonged AP duration (APD) or reduced repolarization reserve, due either to an increase in inward currents or decrease in outward currents, which promotes L-type Ca^{2+} current (I_{Ca}) recovery from inactivation and subsequent reactivation, forming the EAD upstroke (Fig. 7A). The imbalance between inward and outward currents can be caused by direct changes in sarcolemmal ion transport, or by discoordinated Ca^{2+} handling, leading to spontaneous sarcoplasmic reticulum (SR) Ca^{2+} release and subsequent increase in inward Na^+/Ca^{2+} exchange (NCX) current (I_{NCX}), as in delayed afterdepolarizations (DADs, see Fig. 7B–C). Either way, I_{Ca} eventually carries the majority of inward charge contributing to the afterdepolarization upstroke [1].

Recently, we described a novel and unique mechanism underlying phase-3 EADs (Fig. 7D) in ventricular myocytes from arrhythmia-susceptible mice overexpressing Ca^{2+}/calmodulin-dependent protein kinase II (CaMKII) [2]. EADs appearing during β-adrenergic stimulation in these mouse myocytes initiated at membrane potentials negative to −45 mV, and were thus incompatible with reactivation of I_{Ca}. These events also required intact SR Ca^{2+} release but generally occurred prior to or at the same time as the peak of the triggered Ca^{2+} transient, and thus were not driven by secondary spontaneous SR Ca^{2+} release during repolarization [2]. Computational modeling revealed that these EADs were initiated by non-equilibrium reactivation of fast Na^+ current (I_{Na}), not late I_{Na}, and were secondary to enhanced SR Ca^{2+} release and augmented I_{NCX} that held voltage at a negative late plateau [2]. This was confirmed experimentally by the observation that 10 μM ranolazine, which selectively inhibits late I_{Na} in ventricles, did not prevent EAD initiation, whereas tetrodotoxin eliminated EADs [2] at a dose (1 μM) sufficient for approximately half inhibition of peak I_{Na} and 30% inhibition of late I_{Na}. By imposing different voltage waveforms on the Na^+ channel model, we confirmed that specific E_m dynamics (e.g., rapidly repolarizing ramps) permit non-equilibrium reactivation, as opposed to an equilibrium component (e.g., window current) that would emerge after holding the voltage for a prolonged time [2].

This mechanism involving Ca^{2+}-driven non-equilibrium I_{Na} reactivation is permitted by two key characteristics of the murine AP: a triangular repolarization trajectory with short and negative plateau phase (which hastens I_{Na} recovery from inactivation), and a repolarization phase that is strongly modulated by SR Ca^{2+} release and inward I_{NCX}. Thus, phase-3 EADs driven by non-equilibrium I_{Na} gating may constitute a novel mechanism of triggered arrhythmia in cardiac cell types known to exhibit these characteristics, including human atrial myocytes. Indeed, a mechanism involving phase-3 EADs driven by SR Ca^{2+} release and I_{NCX} has been shown to initiate triggered activity and re-induce atrial fibrillation (AF) in isolated canine atria (see Fig. 7E) and pulmonary vein (PV) sleeves during combined sympathetic and parasympathetic stimulation [3–5]. An interaction of both sympathetic and parasympathetic systems is thought to underlie the initiation of clinical AF in humans [6–8] and dogs [9, 10].

Here we sought to determine whether these dynamics may be relevant to the human atrium, where the relatively brief atrial AP and negative AP plateau may permit I_{Na} reactivation events. Indeed, without any parameter adjustment, we replicated phase-3 EADs *in silico* using our established human atrial cell model with updated I_{Na} description (see Methods). Further, we tested the hypothesis that ranolazine, which blocks both peak and late I_{Na} in atria (as opposed to the late I_{Na} selectivity in ventricles) [11–13] and suppresses AF by prolonging the effective refractory period [14], can also prevent phase-3 EAD-mediated triggered activity.

METHODS

We integrated a Markov formulation of I_{Na} [15, 16] into our model of human atrial myocyte electrophysiology and Ca^{2+} cycling [17]. We further expanded the I_{Na} Markov model to describe the interaction of the Na^+ channel with ranolazine, using the approach introduced

by the Clancy group [18, 19]. Based on the assumption that the channel can reside in any state in drug-free or drug-bound conditions, the new model structure is characterized by drug-free and drug-bound layers, as shown in Fig. 1. Transitions between layers were initially modeled as done by Moreno *et al* [19], and transitions within the drug-bound layer were modified relative to the drug-free layer as in [19]. Several voltage-clamp protocols were simulated for parameterization of the ranolazine-I_{Na} model at room temperature: activation, steady-state inactivation, recovery from inactivation, tonic block of peak and late I_{Na}, use-dependent block (UDB), and recovery from UDB. A detailed description of the parameter identification process can be found in [19]. In our implementation, minor parameter adjustments were required to account for the different inactivation scheme in our Markov model *vs.* that used in [19]. Specifically, we modified the transitions between states IF and IM_1 in the drug-bound layer to match the frequency-dependence of UDB observed in experiments. The ranolazine-dependent tonic block of the delayed rectifier K^+ current (I_{Kr}) was also integrated as in [19]. Current-clamp experiments were simulated at 37°C (the Q_{10} for scaling I_{Na} kinetics was 2.1 [20]) to assess the occurrence of EADs with or without ranolazine in the presence of isoproterenol (ISO) and/or acetylcholine (ACh), modeled using the methods of Grandi *et al* [17]. All simulations were performed in MATLAB (The MathWorks, Natick, MA, USA) using the stiff ordinary differential equation solver ode15s. The model code is available for download at the following webpage: somapp.ucdmc.ucdavis.edu/Pharmacology/bers.

RESULTS

Burashnikov and Antzelevitch [5] observed the development of phase-3 EADs after spontaneous termination of AF in canine atrial tissue (Fig. 2A). Under similar conditions (ACh-abbreviated AP, in absence of sympathetic stimulation), our model exhibited a similar slowing of phase-3 repolarization (Fig. 2B, top panel) upon returning from rapid pacing (10 Hz) to sinus rhythm (1 Hz). This effect is due to pause-induced increase in SR Ca^{2+} release and, consequently, enhanced inward I_{NCX}. In fact, Ca^{2+} accumulation in the cell during the fast pacing interval resulted in a transient period of hypercontractility immediately after return to normal sinus rhythm (Fig. 2B, bottom). Increased Ca^{2+} extrusion via NCX contributes to generating the inward current responsible for AP plateau prolongation, i.e., as observed in mouse [2]. Beat by beat, SR Ca^{2+} load decreased, leading to a gradual reduction of the Ca^{2+} transient amplitude (Fig. 2C, right) and I_{NCX}, which caused progressive AP shortening (Fig. 2C, left).

Heart rate variability analysis in human patients [6–8] and nerve activity recordings in ambulatory dogs [9, 10] indicated that the onset of AF is associated with simultaneous discharge of both sympathetic and para-sympathetic limbs, rather than by either vagal or sympathetic activity alone. Consistently, experimental studies involving autonomic nerve stimulation [4], or exogenous agonists [3], suggest that combined sympathetic and parasympathetic challenge is capable of eliciting phase-3 EADs and triggered activity. To emulate experimental protocols, we paced our atrial cell model rapidly (10 Hz), while simulating combined administration of ACh (0.1 μM) and ISO (1 μM). Again, simulations predicted a transient increase in Ca^{2+} transient amplitude after return to sinus rhythm (1 Hz pacing) due to augmented SR Ca^{2+} loading and release (Fig. 3). This enhances I_{NCX}, which

favors AP prolongation and recruits non-equilibrium I_{Na} reactivation via the canonical gating mode (O), thus leading to the development of phase-3 EADs (Fig. 3, asterisks). In Fig. S1 we confirmed that during rapid repolarization ramps total I_{Na} (Fig. S1B, black/red traces) is carried mainly by a non-equilibrium component, because this is already substantial at E_m (and times) where the theoretically maximal equilibrium (window) current of I_{Na} is virtually absent (Fig. S1C, black/red traces). These results extend our observations in murine ventricles [2], and confirm that non-equilibrium I_{Na} reactivation is a likely arrhythmia mechanism in human atrial cells.

We performed additional simulations to assess the likelihood of these EADs to occur and determine the factors that most markedly affect EAD formation. We varied ion channel conductances and maximal transport rates by +/- 3–5% and assessed the occurrence of EADs using the protocol in Fig. 3 (Table S1). As expected, we found EAD initiation to be especially sensitive to I_{Na} conductance. Changes in ACh (analyzed in 5-nM increments) or ISO doses, duration of rapid pacing (1-s increments) duration of the pause (50-ms decrements), also affect EAD occurrence by modulating the repolarization rate or I_{Na} availability. Specifically, starting from the original base-case parameter configuration, [ACh] higher than 135 nM, rapid pacing protocols longer than 23 s, or pauses shorter than 800 ms prevent EADs in the model, primarily by increasing repolarization rate, reducing I_{Na} availability, or both affecting Ca^{2+} loading and I_{Na}, respectively. While ISO effects in this model are simulated as static on/off switches, rather than graded dose-dependent responses, we expect lower [ISO] to result in reduced Ca^{2+} loading, and hence reduced EAD propensity.

We also attempted to replicate this EAD mechanism by another established atrial cell model, and repeated some of the simulations with the Koivumäki *et al* model [21]. We were unable to recapitulate frank EADs as seen in experiments and in our model, and reasoned that this may be due to fundamental differences in model construction. For example, a large difference in stability of intracellular Na^+ markedly diminishes the potential for Ca^{2+} overload to generate “plateau” inward I_{NCX} in the Koivumäki *et al* model. Specifically, we could reproduce data similar to our simulations in Fig. 2 when reducing intracellular Na^+, including our Markov I_{Na} model, and using the Grandi *et al* NCX formulation (not shown).

Our previous study showed that tetrodotoxin blockade of peak I_{Na} prevented this pro-arrhythmic I_{Na} reactivation in mouse ventricular cardiomyocytes [2], whereas specific block of late I_{Na} by ranolazine failed to prevent EAD initiation [2] though APD was shortened. Ranolazine is an open-state Na^+ blocker that unbinds rapidly from the closed state, but stays trapped and cannot unbind from inactivated Na^+ channels. The more depolarized resting E_m of atrial compared with ventricular myocytes (~10 mV more positive) is responsible for a larger fraction of inactivated Na^+ channels in atrial *vs.* ventricular cells (e.g., the fraction of inactivated states increases about 3.5-fold from −85 to −75 mV, dashed lines in Fig. 4C), which makes ranolazine an atrial-selective blocker of peak I_{Na} [12, 13]. Thus, we sought to test whether ranolazine can prevent arrhythmogenic non-equilibrium I_{Na} reactivation in atrium. To pursue this goal, we extended our I_{Na} model to reproduce the experimentally observed consequences of ranolazine-Na^+ channel interaction [15, 19, 22–24]. Ranolazine (10 μM) reduced atrial peak current (Fig. 4A) without altering the voltage-dependence of I_{Na}

activation (Fig. 4B), negatively shifted steady-state inactivation (Fig. 4C), and slowed recovery from inactivation (not shown) [24]. Ranolazine-induced tonic block is higher for late *vs.* peak I_{Na}: simulated IC_{50} values of 7 and 200 μM for late and peak components, respectively, were in good agreement with experimental data (Fig. 4D). In response to repetitive depolarizations, ranolazine caused UDB of peak I_{Na}, which increased with both drug dose (Fig. 4E) and stimulation frequency (Fig. 4F). Recovery from UDB was also slowed by ranolazine administration (not shown) [19].

To test whether ranolazine can prevent phase-3 EAD occurrence in our atrial model, we repeated the simulation shown in Fig. 3 with the addition of various concentrations of the drug. Model outputs were qualitatively similar when simulating ranolazine doses within the therapeutic range (1–10 μM): despite Ca^{2+} overload and enhanced I_{NCX}, ranolazine administration prevented non-equilibrium I_{Na} reactivation and phase-3 EADs were suppressed. Results obtained with 5 μM ranolazine are reported in Fig. 5.

Our results confirm the hypothesis that ranolazine administration can prevent non-equilibrium I_{Na} reactivation because it blocks peak I_{Na} in atrial (but not in ventricular) myocytes. This atrioventricular difference in pharmacological outcome is due to the property of this drug to stay trapped to inactivated Na^+ channels. Since atrial cells are more depolarized at resting E_m (*vs.* ventricular myocytes), more Na^+ channels are inactivated in atrial *vs.* ventricular cells, leading to stronger peak I_{Na} block [11–13]. To quantify this, we applied a triangular ("atrial-like") voltage command (Fig. 6A) to our human atrial model. Administration of 10 μM ranolazine caused a 28% reduction of peak I_{Na} (Fig. 6B) if the cell was held at the typical atrial resting E_m of −75 mV. When holding the resting potential more negative (−85 mV), as in ventricular myocytes, this I_{Na} block was much less (14%). Analogously, both tonic (Fig. 6C) and UDB (Fig. 6D) induced by 10 μM ranolazine were enhanced by about 4-fold when simulating a depolarized resting E_m (−80 mV *vs.* −100 mV in Fig. 4). Thus, it is not surprising that ranolazine exerts its anti-arrhythmic effect at relative low concentrations (1–5 μM). These observations confirm that the more depolarized resting E_m in atrial *vs.* ventricular myocytes plays a pivotal role in determining the ranolazine effect on I_{Na} peak in the two different cardiac tissues.

DISCUSSION

A mechanism for phase-3 EADs involving Ca^{2+}-driven non-equilibrium I_{Na} reactivation is shown here to be relevant in human atrial myocytes, which exhibit an AP morphology that is intermediate to the ventricular APs of the mouse and large mammals. The mechanisms of EAD takeoff at these negative E_m are independent of I_{Ca} reactivation and result from enhanced triggered (not spontaneous) Ca^{2+} release, which subsequently drives NCX-induced prolongation of the (negative) AP plateau after rapid early repolarization (Fig. 7D).

In healthy ventricular myocytes of large mammals, arrhythmogenic non-equilibrium I_{Na} reactivation is hindered by the higher AP plateau and the increased APD, which cause accumulation of channels in the slow-recovering inactive states. However, we speculate that it might become relevant in those pathological conditions in which these AP features are drastically altered. An example may be ischemia-induced remodeling, where resting E_m is

depolarized and APD is shortened. In a pacing-induced rabbit heart failure model, post-shock APD shortening and Ca^{2+} elevation induced recurrent ventricular fibrillation by promoting phase-3 EADs and triggered activity [25]. Post-shock phase-3 EADs were also obtained in Langendorff-perfused hypokalemic rabbit ventricles, when ventricular fibrillation was induced during sympathetic activation [26].

In canine atrial preparations, Burashnikov and Antzelevitch have shown that phase-3 EADs arise after AF termination, and are the trigger for re-induction of fibrillation [5] (Fig. 7E). Analogous triggered phenomena have been described in canine PVs with autonomic nerve stimulation [3], or combined ACh and epinephrine challenge [4]. These protocols mimic simultaneous sympathovagal discharges that commonly precede AF onset [6–10, 27]. Our atrial simulations are consistent with the results of these studies, and capture both the relatively subtle EADs accompanying rapid pacing and ACh (Fig. 2), and the more pronounced depolarizations observed with additional β-adrenergic challenge (Fig. 3). This graded induction from AP prolongation through to clear EADs is a feature of the progressive Ca^{2+} loading accompanying these stimuli [4], and as in our murine experiments [2], results from exaggerated SR Ca^{2+} release and I_{NCX} [4, 5]. Nevertheless, some variability in shape and take-off potential and timing exists in experimentally measured EADs. Figure S2A illustrates the development of ACh- and high Ca^{2+}-induced late phase-3 EADs in PV [28] and superior vena cava [29] sleeve preparations. Late phase-3 EADs are observed at slow rates in beats immediately after rapid pacing and occur at variable take-off potentials (ranging from ~−70 to −45 mV). Our simulated EADs initiate at the depolarized end of this range. By performing sensitivity analysis (Table S1), we also found that relatively small changes in I_{Ca} conductance could uniquely produce relatively large variations in EAD morphology (take-off potential and timing, Fig. S2B). We did not see EADs originating at more negative E_m, although these are also consistent with reactivation of I_{Na}. EAD timing is not markedly different between the model and experiments, and in both it generally occurs at the time of greatest triangulation in trajectory, when I_{Na} is most apt to reactivate i.e. the phase-2/phase-3 transition. Nevertheless, small discrepancies in experimental *vs.* simulated EAD timing might have technical or physiological explanations. Technically, it is possible that in some recordings the microelectrodes are slightly spatially removed from the site of earliest EAD reactivation, and therefore there is some slight delay due to conduction. Physiologically, the temporal offset could be explained by slowing of repolarization due to intracellular Ca^{2+} waves, as occurs in ventricular myocytes during specific conditions of Ca^{2+} overload [30]. Whether it is this or conventional systolic Ca^{2+} release that is responsible for delaying repolarization here, importantly our simulations suggest the novel interpretation that induction of non-equilibrium I_{Na} dynamics is the critical end point of this EAD mechanism, and is therefore responsible for reinitiating AF in these models. In line with this contention, AP-clamp experiments in pig atrial myocytes confirmed that an EAD-shaped voltage command elicited a lidocaine-sensitive (20–200 μM) inward current compatible with simulated I_{Na} dynamics (not shown), similar to results in murine ventricles [2]. An important qualifier for this interpretation is that the experimental protocols involving ACh challenge also facilitate I_{Na} reactivation by shortening the AP. However, AP shortening and EADs of this type can also be induced by autonomic nerve stimulation without exogenous agonists [3], and it is known that simultaneous parasympathetic and sympathetic

activation may precede AF onset [27]. Note that ACh will tend to cause E_m hyperpolarization (from ~−76 mV to ~−82 mV with 1 μM ACh in our simulations).

Our local sensitivity analysis involved modest perturbations in ionic conductances to support the concept that EADs are not especially sensitive to parameters other than I_{Na} while limiting the influence on overall model behavior (e.g., maintaining AP and Ca^{2+} transient properties close to the original base-case model). Future studies could exploit more informative techniques for parameter sensitivity analysis (and larger variations), which have been recently applied in computational electrophysiological and Ca^{2+} handling models [31–35].

PVs play a particularly important role in paroxysmal AF (pAF) patients [36], and there is evidence that PV cardiomyocytes possess properties predisposing to both Ca^{2+}-driven focal activity and reentry. While it is possible that both DADs and EADs contribute to PV ectopy, based on data from models of acute AF, and data describing the early electrophysiological changes in AF [37], we contend that EADs are a likely source of ectopy early in disease progression. Specifically, we speculate that the short PV AP, and late AP plateau (at negative E_m) induced by autonomic challenge, can facilitate non-equilibrium I_{Na} reactivation at negative plateau E_m, late during repolarization, as we have shown in our computational human atrial myocytes (Fig. 3) and in mouse ventricular myocytes [2]. In an arrhythmia-susceptible canine model, Ca^{2+} transient amplitude and kinetics were similar in myocytes from both PVs and atrium [38], which supports the contention that what we have seen in the human atrial model might also hold true in PVs.

If our proposed mechanism proves to be an important initiator of atrial and PV ectopy, it may assist development of more effective pharmacotherapeutics, e.g., evaluating the efficacy and safety of class 1C antiarrhythmic drugs for treatment of pAF treatment. Indeed, flecainide (a potent I_{Na} blocker and effective anti-AF drug) is contraindicated in patients with heart failure, because of a high risk of induction of ventricular arrhythmia [39]. By revealing the mechanisms of drug efficacy and atrial selectivity, our computational approach might facilitate more specific drug development pipelines [40, 41]. In a recent study, a computational modeling approach informed and validated by experimental data has been developed to simulate the interaction kinetics of the antiarrhythmic drugs flecainide and lidocaine with cardiac Na^+ channels (Fig. 1, [18]). More recently, this framework has been extended to simulate the novel Na^+ channel blocker ranolazine, which preferentially blocks late *vs.* peak I_{Na} in ventricles, but also blocks hERG current I_{Kr} with therapeutic concentrations resulting in QTc prolongation. Ranolazine is contraindicated for patients with preexisting QT prolongation, but we have examined its effectiveness in diverse arrhythmia-provoking contexts characterized by enhancement of late I_{Na} [19]. Ranolazine cannot unbind from inactivated Na^+ channels. The fraction of inactivated channels is greater in atrial *vs.* ventricular myocytes, as a result of the more negative Na^+ channel steady-state inactivation curve (in some species) and the more depolarized resting E_m. This confers ranolazine atrial selectivity (compared with ventricles) for peak I_{Na} block [11–13]. Accordingly, our computational analysis showed that a depolarized resting E_m enhances the ranolazine-induced tonic block of peak I_{Na} (Fig. 6A–C). Moreover, because much of the recovery from Na^+ channel block occurs from non-inactivated states of the channel, atrial cells show a

greater accumulation of use-dependent Na^+ channel block (Fig. 6D). Notably, ranolazine suppresses AF by prolonging the effective refractory period via an increase in post-repolarization refractoriness [14], and has been shown to suppress experimentally measured phase-3 EADs in PV sleeves, via its actions to reduce $[Ca^{2+}]_i$ secondary to changes in I_{Na} and late I_{Ca} [28]. Here, we show that ranolazine can also suppress EAD-mediated ectopic activity in atrial myocytes by significantly reducing non-equilibrium I_{Na} reactivation (Fig. 5). This is achieved in our model simply due to a depolarized atrial resting E_m, as differences in I_{Na} availability have been ruled out in human atrial *vs.* ventricular myocytes [42]. We speculate that ranolazine may be even more efficacious and selective for PV myocytes, given their even more depolarized resting E_m [43].

It is well known that ranolazine targets multiple mechanisms in cardiac cells. As done previously [19], our Markov I_{Na} model accounts for both the fast and the late I_{Na} (and so does the drug model). I_{Kr} block is incorporated as well, although it was shown to not appreciably affect atrial APD ([17], confirmed by experiments by Wettwer *et al* [44]), or even greatly potentiate atrial-selective I_{Na} block [14]. It has also been reported that ranolazine directly influences ryanodine receptor (RyR) open probability and desensitizes Ca^{2+}-dependent RyR activation [45]. However, we did not see any significant effect of ranolazine (10 μM) on myocytes Ca^{2+} sparks and SR Ca^{2+} load in permeabilized mouse ventricular myocytes (not shown). In addition to direct ranolazine effects on these channels, which warrant further investigation, our previous modeling work supports the notion that ranolazine may act to desensitize RyRs indirectly by normalizing intracellular Na^+ loading and decreasing CaMKII-dependent RyR phosphorylation [46]. In fact, reduction of late I_{Na} by ranolazine and GS-458967, a more selective and potent inhibitor of late I_{Na}, also reduces the incidence of DADs in experimental studies of PV and superior vena cava sleeves [29, 47] potentially by reducing Na^+ and hence Ca^{2+} loading. Importantly, simulations of other Na^+ channel blockers (flecainide, lidocaine, which does not inhibit I_{Kr}, and GS-458967) may help define the necessary E_m- and time-dependent characteristics of Na^+ channel block that ensure atrial selectivity of peak I_{Na} blockade, as well as the consequences of off-target effects.

CONCLUSIONS

Our study unveils non-equilibrium I_{Na} reactivation as a novel arrhythmia mechanism in human atrial myocytes, as previously observed in mouse ventricular cells [2]. These cardiac cell types are both characterized by a triangular repolarization trajectory with short and negative plateau, and a late phase of repolarization strongly dependent on SR Ca^{2+} release and inward I_{NCX}. The negative AP plateau hastens I_{Na} recovery from inactivation, which can then reactivate when the AP is prolonged by increased Ca^{2+} extrusion via NCX, leading to phase-3 EAD initiation. We showed that pharmacological inhibition of peak I_{Na} can prevent this pro-arrhythmic mechanism in both atrial and ventricular cells. The more depolarized resting E_m in atrial (*vs.* ventricular) myocytes confers atrial selectivity for peak I_{Na} block to the Na^+ channel blocker ranolazine [11–13], which prevents the arrhythmogenic reactivation of I_{Na} in atrial cells but not in ventricular myocytes. Our findings suggest that this pro-arrhythmic mechanism may be relevant also in human PVs, where the more depolarized resting E_m (*vs.* atrial free-wall cells) may further increase the efficacy of ranolazine

treatment. Taken together, these observations corroborate the concept of atrial-selective inhibition of peak I_{Na} as a promising therapeutic strategy for the management of AF [11, 14, 41].

Supplementary Material

Refer to Web version on PubMed Central for supplementary material.

ACKNOWLEDGEMENTS

This work was supported by a Postdoctoral Fellowship (2014POST18380011, SM) and a Scientist Development Grant (15SDG24910015, EG) from the American Heart Association, and NIH Grant R01-HL105242 (DMB & ADM). We are grateful to Dr. Hitoshi Uchinoumi for sharing unpublished results on the effects of ranolazine on Ca^{2+} sparks, to Drs. Colleen Clancy and Pei-Chi Yang for sharing the code of their I_{Na} Markov model, and to Dr. Jussi Koivumäki for sharing the code of his atrial model.

Abbreviations

ACh	acetylcholine
AF	atrial fibrillation
AP	action potential
APD	action potential duration
$[Ca^{2+}]_i$	intracellular Ca^{2+} concentration
CaMKII	Ca^{2+}/calmodulin-dependent protein kinase II
DAD	delayed afterdepolarization
EAD	early afterdepolarization
E_m	membrane potential
I_{Ca}	L-type Ca^{2+} current
I_{Na}	Na^+ current
I_{Kr}	delayed rectifier K^+ current
I_{NCX}	Na^+/Ca^{2+} exchanger current
ISO	isoproterenol
NCX	Na^+/Ca^{2+} exchanger
pAF	paroxysmal atrial fibrillation
PV	pulmonary vein
RyR	ryanodine receptor
SR	sarcoplasmic reticulum
UDB	use-dependent block

REFERENCES

1. Weiss JN, Garfinkel A, Karagueuzian HS, Chen PS, Qu Z. Early afterdepolarizations and cardiac arrhythmias. Heart Rhythm. 2010; 7:1891–1899. [PubMed: 20868774]
2. Edwards AG, Grandi E, Hake JE, Patel S, Li P, Miyamoto S, et al. Non-equilibrium reactivation of the Na+ current drives early afterdepolarizations in mouse ventricle. Circ Arrhythm Electrophysiol. 2014; 7:1205–1213. [PubMed: 25236710]
3. Patterson E, Lazzara R, Szabo B, Liu H, Tang D, Li YH, et al. Sodium-calcium exchange initiated by the Ca2+ transient: an arrhythmia trigger within pulmonary veins. J Am Coll Cardiol. 2006; 47:1196–1206. [PubMed: 16545652]
4. Patterson E, Po SS, Scherlag BJ, Lazzara R. Triggered firing in pulmonary veins initiated by in vitro autonomic nerve stimulation. Heart Rhythm. 2005; 2:624–631. [PubMed: 15922271]
5. Burashnikov A, Antzelevitch C. Reinduction of atrial fibrillation immediately after termination of the arrhythmia is mediated by late phase 3 early afterdepolarization-induced triggered activity. Circulation. 2003; 107:2355–2360. [PubMed: 12695296]
6. Amar D, Zhang H, Miodownik S, Kadish AH. Competing autonomic mechanisms precede the onset of postoperative atrial fibrillation. J Am Coll Cardiol. 2003; 42:1262–1268. [PubMed: 14522493]
7. Bettoni M, Zimmermann M. Autonomic tone variations before the onset of paroxysmal atrial fibrillation. Circulation. 2002; 105:2753–2759. [PubMed: 12057990]
8. Tomita T, Takei M, Saikawa Y, Hanaoka T, Uchikawa S, Tsutsui H, et al. Role of autonomic tone in the initiation and termination of paroxysmal atrial fibrillation in patients without structural heart disease. J Cardiovasc Electrophysiol. 2003; 14:559–564. [PubMed: 12875412]
9. Tan AY, Zhou S, Ogawa M, Song J, Chu M, Li H, et al. Neural mechanisms of paroxysmal atrial fibrillation and paroxysmal atrial tachycardia in ambulatory canines. Circulation. 2008; 118:916–925. [PubMed: 18697820]
10. Ogawa M, Zhou S, Tan AY, Song J, Gholmieh G, Fishbein MC, et al. Left stellate ganglion and vagal nerve activity and cardiac arrhythmias in ambulatory dogs with pacing-induced congestive heart failure. J Am Coll Cardiol. 2007; 50:335–343. [PubMed: 17659201]
11. Antzelevitch C, Burashnikov A. Atrial-selective sodium channel block as a novel strategy for the management of atrial fibrillation. Ann N Y Acad Sci. 2010; 1188:78–86. [PubMed: 20201889]
12. Burashnikov A, Di Diego JM, Zygmunt AC, Belardinelli L, Antzelevitch C. Atrial-selective sodium channel block as a strategy for suppression of atrial fibrillation. Ann N Y Acad Sci. 2008; 1123:105–112. [PubMed: 18375582]
13. Burashnikov A, Di Diego JM, Zygmunt AC, Belardinelli L, Antzelevitch C. Atrium-selective sodium channel block as a strategy for suppression of atrial fibrillation: differences in sodium channel inactivation between atria and ventricles and the role of ranolazine. Circulation. 2007; 116:1449–1457. [PubMed: 17785620]
14. Burashnikov A, Di Diego JM, Barajas-Martinez H, Hu D, Zygmunt AC, Cordeiro JM, et al. Ranolazine Effectively Suppresses Atrial Fibrillation in the Setting of Heart Failure. Circ Heart Fail. 2014
15. Wagner S, Hacker E, Grandi E, Weber SL, Dybkova N, Sossalla S, et al. Ca/calmodulin kinase II differentially modulates potassium currents. Circ Arrhythm Electrophysiol. 2009; 2:285–294. [PubMed: 19808479]
16. Grandi E, Puglisi JL, Wagner S, Maier LS, Severi S, Bers DM. Simulation of Ca-calmodulin-dependent protein kinase II on rabbit ventricular myocyte ion currents and action potentials. Biophys J. 2007; 93:3835–3847. [PubMed: 17704163]
17. Grandi E, Pandit SV, Voigt N, Workman AJ, Dobrev D, Jalife J, et al. Human atrial action potential and Ca2+ model: sinus rhythm and chronic atrial fibrillation. Circ Res. 2011; 109:1055–1066. [PubMed: 21921263]
18. Moreno JD, Zhu ZI, Yang PC, Bankston JR, Jeng MT, Kang C, et al. A computational model to predict the effects of class I anti-arrhythmic drugs on ventricular rhythms. Sci Transl Med. 2011; 3:98ra83.

19. Moreno JD, Yang PC, Bankston JR, Grandi E, Bers DM, Kass RS, et al. Ranolazine for congenital and acquired late INa-linked arrhythmias: in silico pharmacological screening. Circ Res. 2013; 113:e50–e61. [PubMed: 23897695]
20. Maltsev VA, Undrovinas AI. A multi-modal composition of the late Na+ current in human ventricular cardiomyocytes. Cardiovasc Res. 2006; 69:116–127. [PubMed: 16223473]
21. Koivumaki JT, Seemann G, Maleckar MM, Tavi P. In silico screening of the key cellular remodeling targets in chronic atrial fibrillation. PLoS Comput Biol. 2014; 10:e1003620. [PubMed: 24853123]
22. Sossalla S, Kallmeyer B, Wagner S, Mazur M, Maurer U, Toischer K, et al. Altered Na(+) currents in atrial fibrillation effects of ranolazine on arrhythmias and contractility in human atrial myocardium. J Am Coll Cardiol. 2010; 55:2330–2342. [PubMed: 20488304]
23. Antzelevitch C, Belardinelli L, Zygmunt AC, Burashnikov A, Di Diego JM, Fish JM, et al. Electrophysiological effects of ranolazine, a novel antianginal agent with antiarrhythmic properties. Circulation. 2004; 110:904–910. [PubMed: 15302796]
24. Rajamani S, El-Bizri N, Shryock JC, Makielski JC, Belardinelli L. Use-dependent block of cardiac late Na(+) current by ranolazine. Heart Rhythm. 2009; 6:1625–1631. [PubMed: 19879541]
25. Ogawa M, Morita N, Tang L, Karagueuzian HS, Weiss JN, Lin SF, et al. Mechanisms of recurrent ventricular fibrillation in a rabbit model of pacing-induced heart failure. Heart Rhythm. 2009; 6:784–792. [PubMed: 19467505]
26. Maruyama M, Ai T, Chua SK, Park HW, Lee YS, Shen MJ, et al. Hypokalemia promotes late phase 3 early afterdepolarization and recurrent ventricular fibrillation during isoproterenol infusion in Langendorff perfused rabbit ventricles. Heart Rhythm. 2014; 11:697–706. [PubMed: 24378768]
27. Shen MJ, Zipes DP. Role of the autonomic nervous system in modulating cardiac arrhythmias. Circ Res. 2014; 114:1004–1021. [PubMed: 24625726]
28. Sicouri S, Glass A, Belardinelli L, Antzelevitch C. Antiarrhythmic effects of ranolazine in canine pulmonary vein sleeve preparations. Heart Rhythm. 2008; 5:1019–1026. [PubMed: 18598958]
29. Sicouri S, Blazek J, Belardinelli L, Antzelevitch C. Electrophysiological characteristics of canine superior vena cava sleeve preparations: effect of ranolazine. Circ Arrhythm Electrophysiol. 2012; 5:371–379. [PubMed: 22407414]
30. Zhao Z, Wen H, Fefelova N, Allen C, Baba A, Matsuda T, et al. Revisiting the ionic mechanisms of early afterdepolarizations in cardiomyocytes: predominant by Ca waves or Ca currents? Am J Physiol Heart Circ Physiol. 2012; 302:H1636–H1644. [PubMed: 22307670]
31. Sobie EA. Parameter sensitivity analysis in electrophysiological models using multivariable regression. Biophys J. 2009; 96:1264–1274. [PubMed: 19217846]
32. Sarkar AX, Christini DJ, Sobie EA. Exploiting mathematical models to illuminate electrophysiological variability between individuals. J Physiol. 2012; 590:2555–2567. [PubMed: 22495591]
33. Lee YS, Liu OZ, Hwang HS, Knollmann BC, Sobie EA. Parameter sensitivity analysis of stochastic models provides insights into cardiac calcium sparks. Biophys J. 2013; 104:1142–1150. [PubMed: 23473497]
34. Romero L, Pueyo E, Fink M, Rodriguez B. Impact of ionic current variability on human ventricular cellular electrophysiology. Am J Physiol Heart Circ Physiol. 2009; 297:H1436–H1445. [PubMed: 19648254]
35. Britton OJ, Bueno-Orovio A, Van Ammel K, Lu HR, Towart R, Gallacher DJ, et al. Experimentally calibrated population of models predicts and explains intersubject variability in cardiac cellular electrophysiology. Proc Natl Acad Sci U S A. 2013; 110:E2098–E2105. [PubMed: 23690584]
36. Haissaguerre M, Jais P, Shah DC, Takahashi A, Hocini M, Quiniou G, et al. Spontaneous initiation of atrial fibrillation by ectopic beats originating in the pulmonary veins. N Engl J Med. 1998; 339:659–666. [PubMed: 9725923]
37. Voigt N, Heijman J, Wang Q, Chiang DY, Li N, Karck M, et al. Cellular and molecular mechanisms of atrial arrhythmogenesis in patients with paroxysmal atrial fibrillation. Circulation. 2014; 129:145–156. [PubMed: 24249718]

38. Coutu P, Chartier D, Nattel S. Comparison of Ca2+-handling properties of canine pulmonary vein and left atrial cardiomyocytes. Am J Physiol Heart Circ Physiol. 2006; 291:H2290–H2300. [PubMed: 16798822]

39. Echt DS, Liebson PR, Mitchell LB, Peters RW, Obias-Manno D, Barker AH, et al. Mortality and morbidity in patients receiving encainide, flecainide, or placebo. The Cardiac Arrhythmia Suppression Trial. N Engl J Med. 1991; 324:781–788. [PubMed: 1900101]

40. Aguilar-Shardonofsky M, Vigmond EJ, Nattel S, Comtois P. In silico optimization of atrial fibrillation-selective sodium channel blocker pharmacodynamics. Biophys J. 2012; 102:951–960. [PubMed: 22404917]

41. Aguilar M, Nattel S. The past, present and potential future of sodium channel block as an atrial fibrillation suppressing strategy. J Cardiovasc Pharmacol. 2015

42. Sakakibara Y, Furukawa T, Singer DH, Jia H, Backer CL, Arentzen CE, et al. Sodium current in isolated human ventricular myocytes. Am J Physiol. 1993; 265:H1301–H1309. [PubMed: 8238418]

43. Ehrlich JR, Cha TJ, Zhang L, Chartier D, Melnyk P, Hohnloser SH, et al. Cellular electrophysiology of canine pulmonary vein cardiomyocytes: action potential and ionic current properties. J Physiol. 2003; 551:801–813. [PubMed: 12847206]

44. Wettwer E, Hala O, Christ T, Heubach JF, Dobrev D, Knaut M, et al. Role of IKur in controlling action potential shape and contractility in the human atrium: influence of chronic atrial fibrillation. Circulation. 2004; 110:2299–2306. [PubMed: 15477405]

45. Parikh A, Mantravadi R, Kozhevnikov D, Roche MA, Ye Y, Owen LJ, et al. Ranolazine stabilizes cardiac ryanodine receptors: a novel mechanism for the suppression of early afterdepolarization and torsades de pointes in long QT type 2. Heart Rhythm. 2012; 9:953–960. [PubMed: 22245792]

46. Morotti S, Edwards AG, McCulloch AD, Bers DM, Grandi E. A novel computational model of mouse myocyte electrophysiology to assess the synergy between Na+ loading and CaMKII. J Physiol. 2014; 592:1181–1197. [PubMed: 24421356]

47. Sicouri S, Belardinelli L, Antzelevitch C. Antiarrhythmic effects of the highly selective late sodium channel current blocker GS-458967. Heart Rhythm. 2013; 10:1036–1043. [PubMed: 23524321]

Highlights

- Combined ISO and ACh cause phase-3 EADs in human atrial myocyte simulations
- Phase-3 EADs are favored by increased Ca^{2+} transients and rapid E_m repolarization
- NCX-mediated long AP plateaus recruit non-equilibrium I_{Na} reactivation to favor EAD
- Ranolazine prevents phase-3 EADs in an atrial selective manner

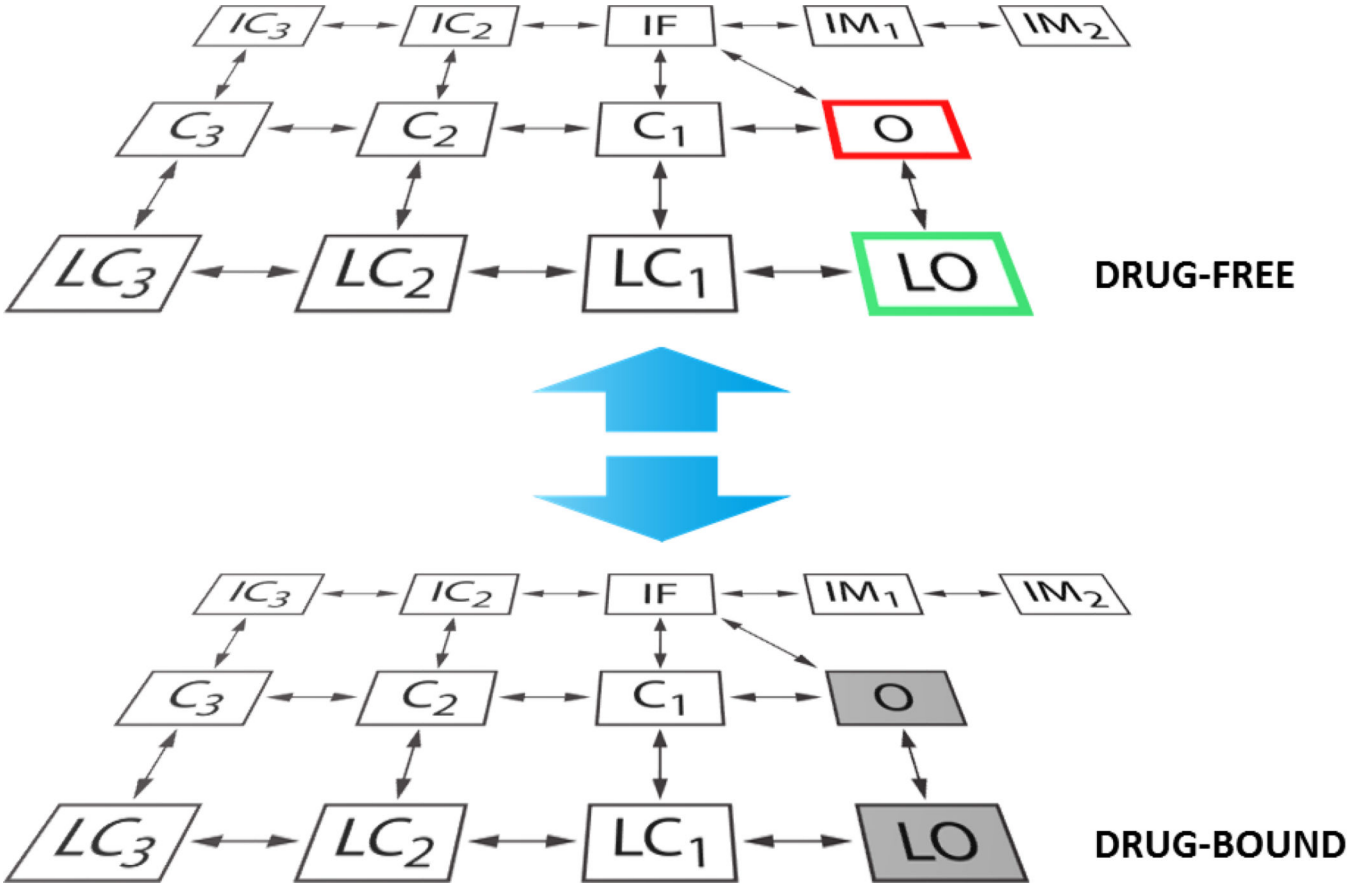

Figure 1. I_{Na} Markov model schematic

When no drug is applied, I_{Na} is modeled with a 13-state Markov scheme [15, 16] accounting for both canonical and burst gating modes (see drug-free layer in figure). O and LO are respectively the conducting open states for normal and burst mode, and C_1-C_3 and LC_1-LC_3 are the corresponding closed states. IF is the fast inactivation state, IM_1-IM_2 represent intermediate inactivation, and IC_2-IC_3 are the deeply inactivated states. To model ranolazine interaction with the Na^+ channel, we used the extended scheme shown here, assuming that the channel can reside in any state in drug-free or drug-bound conditions (as done in [18, 19]). Transitions between layers are E_m- and dose-dependent, and can occur between analogous states only. Ranolazine binding is facilitated when the channel resides in the open states. The drug unbinds rapidly from the closed states, but stays trapped in the inactivated states. O and LO in the drug-bound layer are not conducting states.

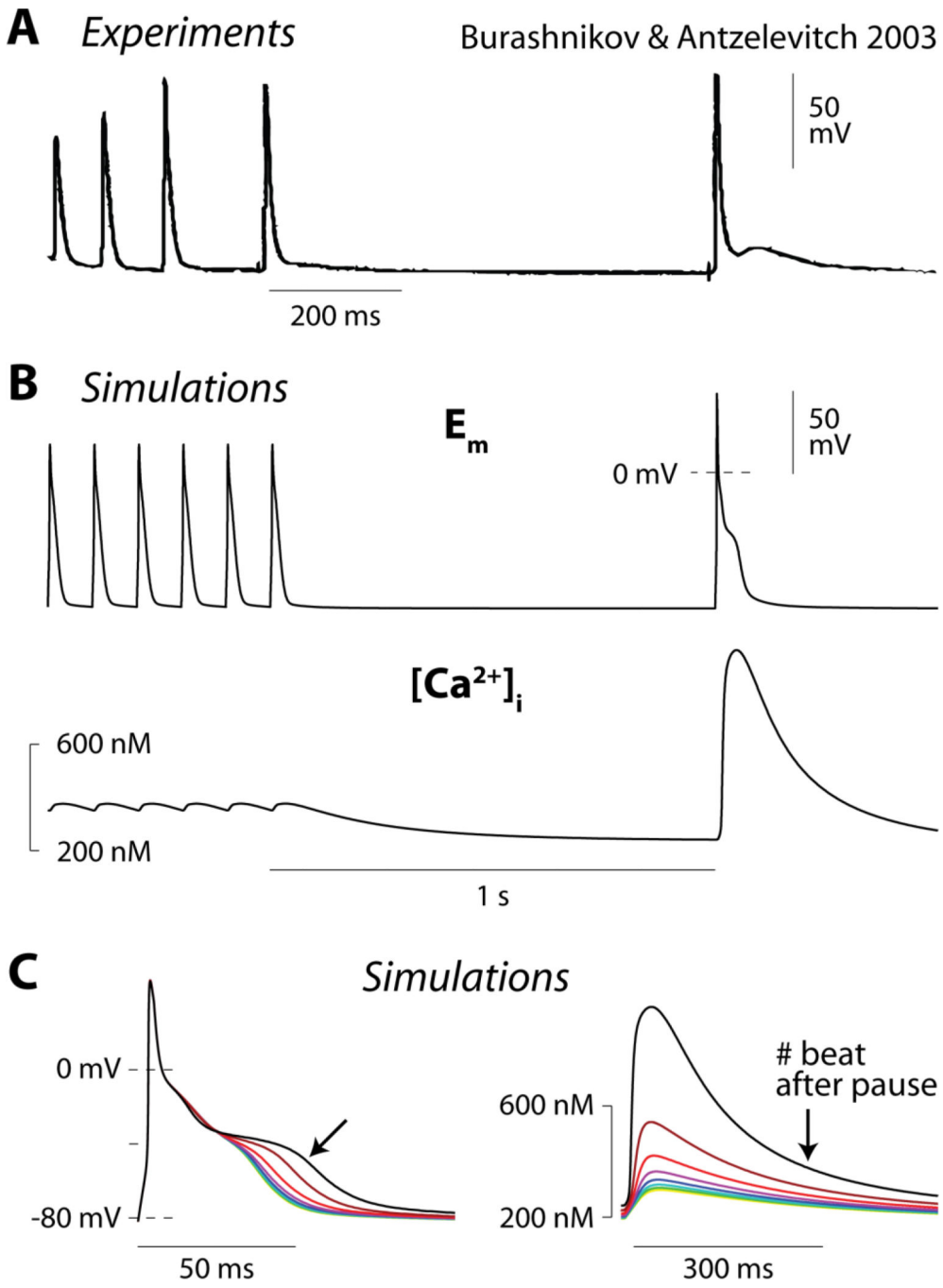

Figure 2. Atrial AP plateau is potently modulated by I_{NCX}

A) A phase-3 EAD is recorded immediately after (first beat after pause) spontaneous termination of AF in isolated canine atrium (reproduced with permission from [5]). **B)** The above experiment is simulated with our human atrial myocyte model. The cell is paced rapidly (10 Hz) for 20 s and then returned to sinus rhythm (1 Hz) in the presence of 1 μM ACh. Time courses of E_m (top) and intracellular Ca^{2+} concentration ($[Ca^{2+}]_i$, bottom) are shown. **C)** Sequence of simulated beats after returning to normal sinus rhythm. AP

progressively shortens (left) due to SR unloading, and diminishes Ca^{2+} transient (right) and I_{NCX}.

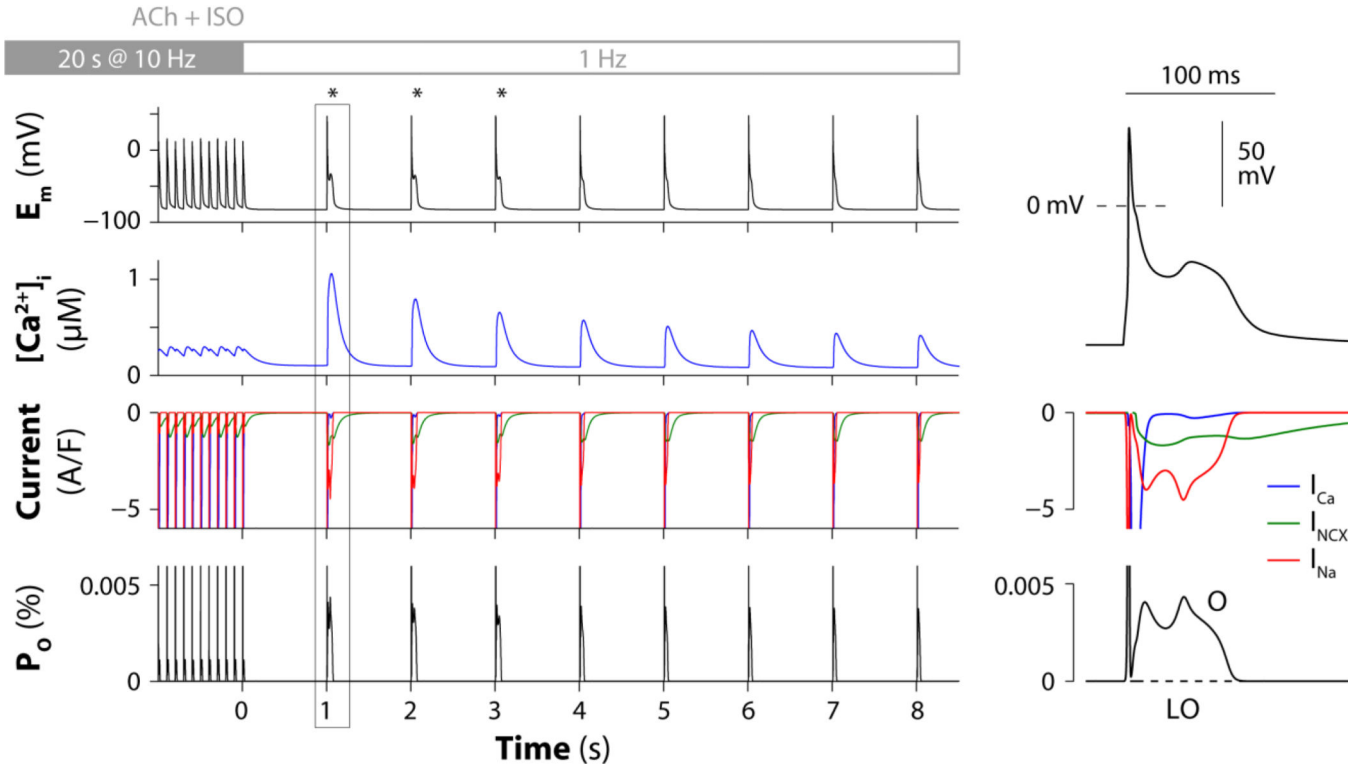

Figure 3. Non-equilibrium I_{Na} reactivation underlies phase-3 EADs in human atrial cells

The digital human atrial myocyte is paced rapidly (10 Hz) for 20 s and then returned to sinus rhythm (1 Hz) in the presence of 0.1 μM ACh and 1 μM ISO. Left panels show the predicted time courses of E_m, $[Ca^{2+}]_i$, I_{Ca}, I_{NCX}, I_{Na}, and occupancies of the I_{Na} model open states (O and LO). A transient period of hypercontractility occurs immediately after return to normal sinus rhythm (second row) because of augmented SR Ca^{2+} loading and release. Enhanced I_{NCX} facilitates I_{Na} reactivation (third row) via the canonical gating mode (bottom). Right panels show magnified traces for the first beat after returning to normal sinus rhythm.

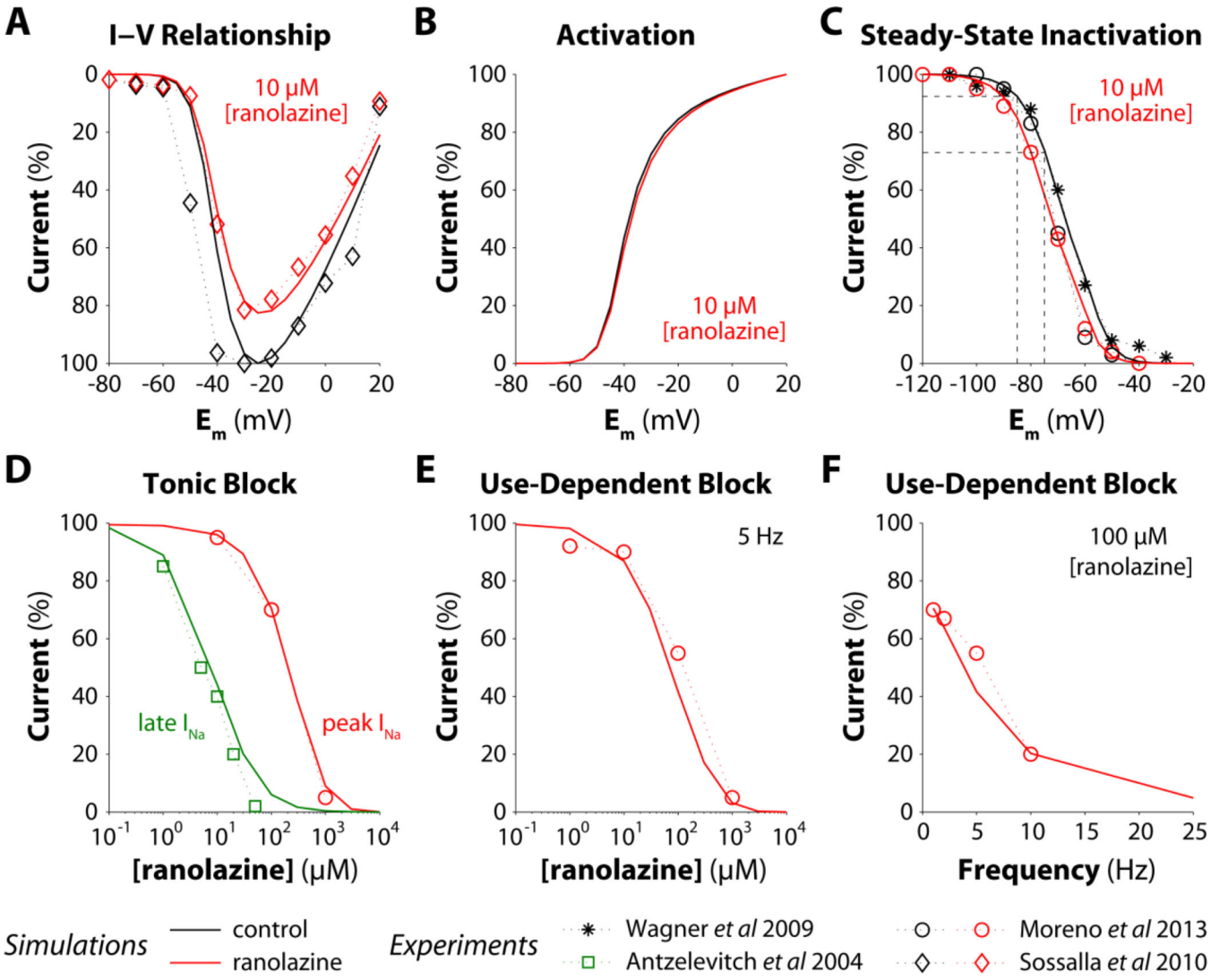

Figure 4. Effects of ranolazine on I_{Na} biophysical properties and properties of block

I_{Na} model parameters are optimized to match simulation outputs (lines) with experiments (symbols, from [15, 19, 22, 23]). **A–C)** Peak I_{Na}-E_m relationship (normalized to maximal peak current in drug-free condition), activation, and steady-state inactivation with or without 10 μM ranolazine. **D)** Dose-dependence of tonic block for peak and late I_{Na} evoked by a 200-ms depolarizing pulse from −100 to −10 mV. Current amplitude in the presence of ranolazine is normalized to the current amplitude in the absence of drug. **E–F)** Dose- and frequency-dependence of UDB from a train of 300 25-ms long pulses (from −100 to −10 mV). I_{Na} amplitude in the presence of ranolazine at the last pulse is normalized to I_{Na} amplitude in drug-free condition.

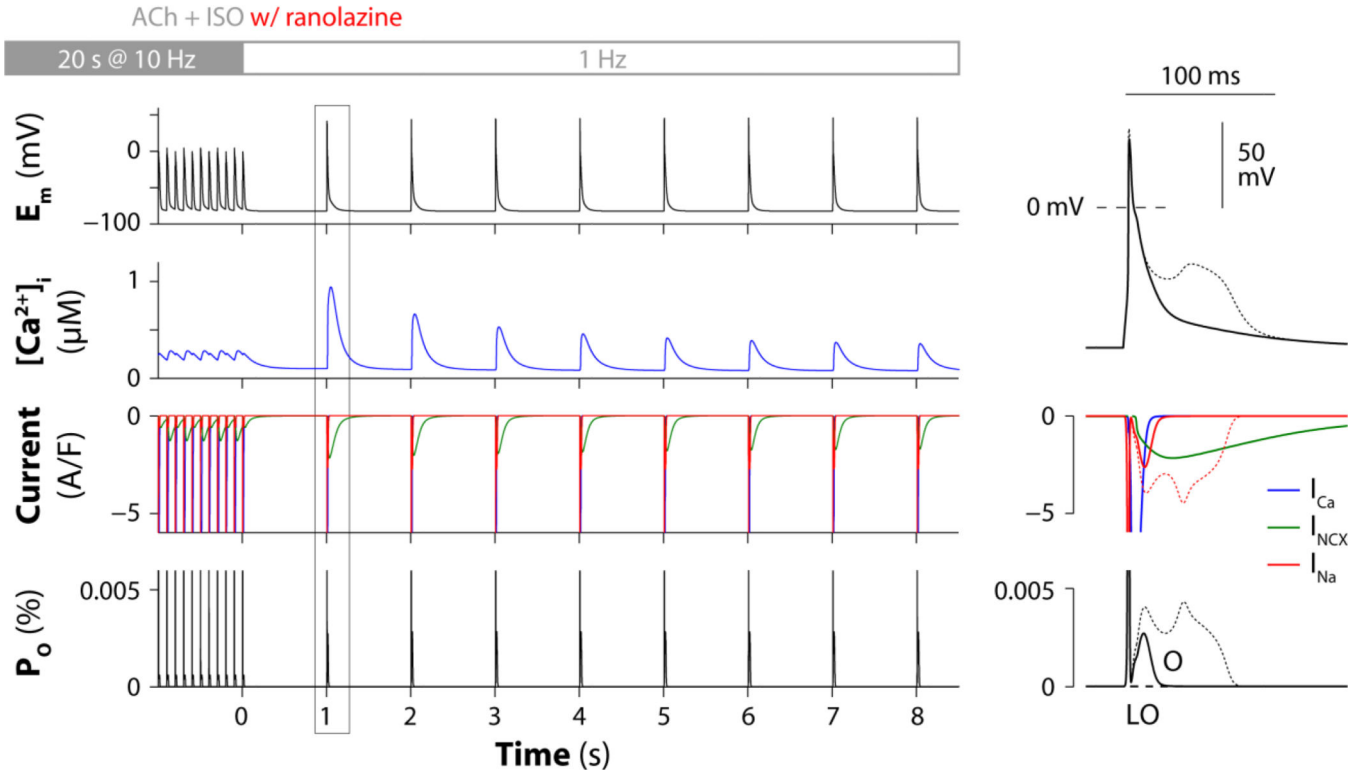

Figure 5. Ranolazine inhibits arrhythmogenic non-equilibrium I_{Na} reactivation

The digital human atrial myocyte is paced rapidly (10 Hz) for 20 s and then returned to sinus rhythm (1 Hz) in the presence of 0.1 μM ACh and 1 μM ISO (as in Fig. 3) and administration of 5 μM ranolazine. Left panels show the predicted time courses of E_m, $[Ca^{2+}]_i$, I_{Ca}, I_{NCX}, I_{Na}, and occupancies of the I_{Na} model open states (O and LO). A transient period of hypercontractility occurs immediately after return to normal sinus rhythm (second row) because of augmented SR Ca^{2+} loading and release. Despite enhanced I_{NCX} (third row), I_{Na} reactivation via the canonical gating mode (bottom) is prevented by ranolazine and EADs are suppressed. Right panels show magnified traces for the first beat after returning to normal sinus rhythm. E_m, I_{Na} and O traces in the absence of ranolazine (from Fig. 3) are reported for comparison (superimposed thin dotted lines).

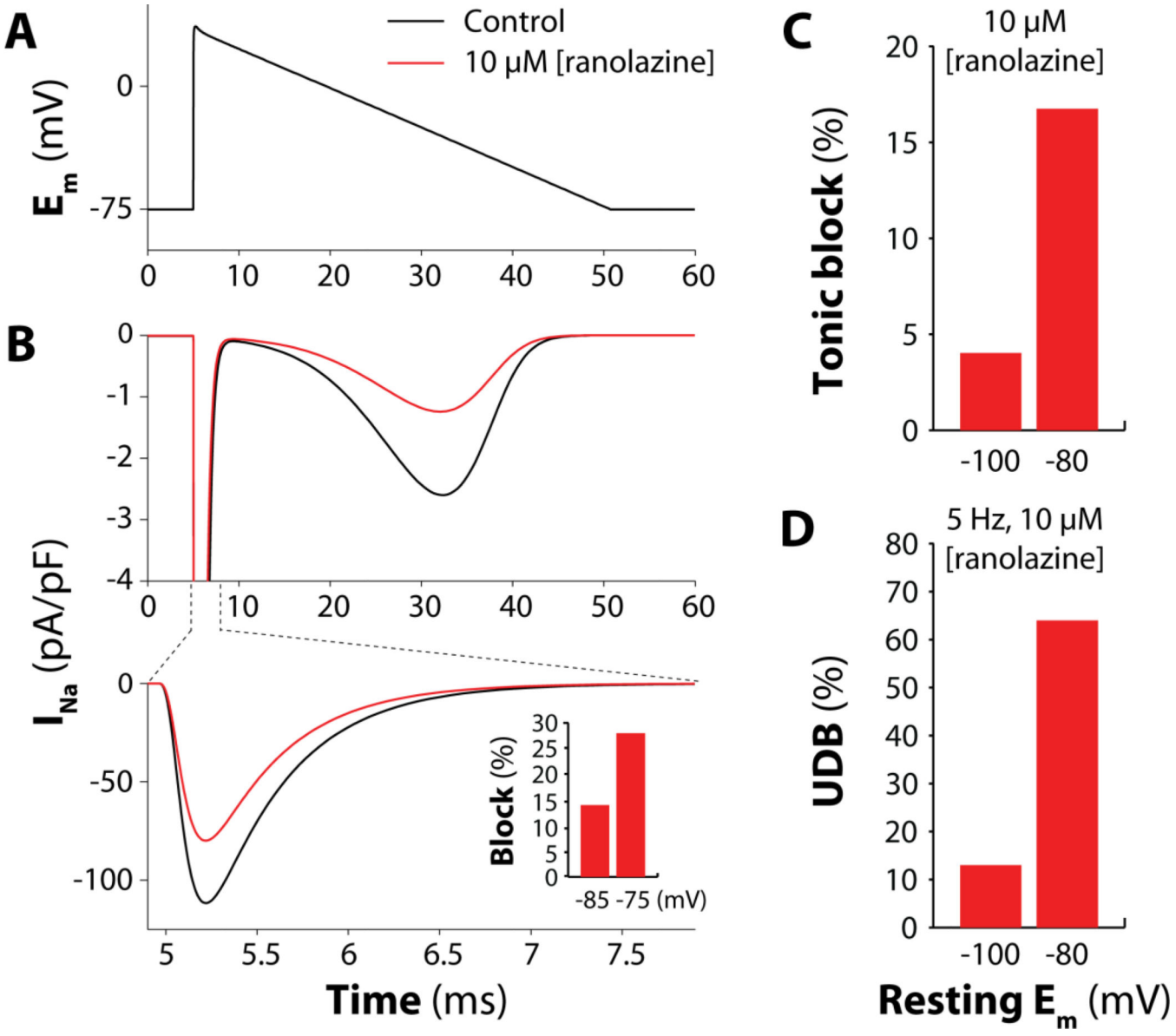

Figure 6. Depolarized resting E_m enhances ranolazine-induced block of peak I_{Na}

A) A triangular voltage command is applied to the digital human atrial myocyte. Resting E_m is −75 mV. **B)** Evoked I_{Na} traces in drug-free condition (control) or in presence of 10 μM ranolazine. Ranolazine reduces peak I_{Na} by 28%, and the current reactivating during the repolarizing ramp by 52%. The more depolarized the resting E_m the larger the peak current block (inset). **C)** Resting E_m-dependence of tonic block for peak I_{Na} with 10 μM ranolazine (obtained replicating the same protocol as Fig. 4D). **D)** Resting E_m-dependence of UDB for peak I_{Na} with 10 μM ranolazine (protocol as Fig. 4E).

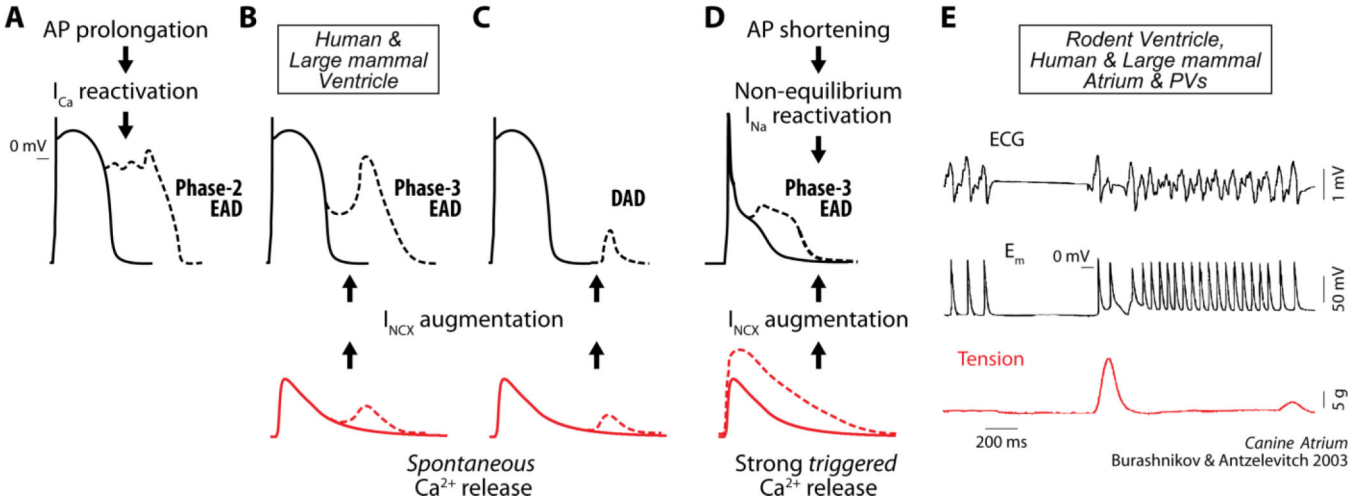

Figure 7. Mechanisms of afterdepolarization formation in cardiomyocytes

In ventricular myocytes from large mammals, phase-2 EADs are associated with I_{Ca} recovery from inactivation and reactivation during prolonged APs (**A**). Spontaneous SR Ca^{2+} release, which increases Ca^{2+} extrusion via NCX (inward current), can lead to phase-3 EADs (**B**) or DADs (**C**) when occurring during or after E_m repolarization respectively. In murine ventricle, phase-3 EADs are favored by potentiated (triggered) Ca^{2+} transient and AP shortening (**D**). The former causes I_{NCX} augmentation and AP plateau prolongation (at negative E_m), during which non-equilibrium I_{Na} reactivation (permitted by rapid I_{Na} recovery during fast repolarization) can occur. This, which is shown here to be relevant in the human atrium, could be a universal mechanism underlying EAD formation in both atria (especially PVs) and ventricles ([26]) of large mammals. Indeed, phase-3 EADs mediate re-initiation of atrial (and ventricular) fibrillation. ECG, E_m and tension recorded in canine atrium (**E**, reproduced with permission from [5]) show phase-3 EADs occurring after termination of fast atrial pacing, which are accompanied by increased contractile force.